

0005 62213723

LIBRARIES MICHIGAN STATE UNIVERSITY EAST LANSING, MICH 48824-1048

This is to certify that the thesis entitled

A PERIODIC LAYERED MEDIUM GREEN'S FUNCTION

presented by

CHRISTOPHER P. TRAMPEL

has been accepted towards fulfillment of the requirements for the

Master of Science

Major Professor's Signature

Nov (6, 2004)

Date

MSU is an Affirmative Action/Equal Opportunity Institution

PLACE IN RETURN BOX to remove this checkout from your record. TO AVOID FINES return on or before date due. MAY BE RECALLED with earlier due date if requested.

DATE DUE	DATE DUE	DATE DUE

6/01 c:/CIRC/DateDue.p65-p.15

A PERIODIC LAYERED MEDIUM GREEN'S FUNCTION

 $\mathbf{B}\mathbf{y}$

Christopher P. Trampel

A THESIS

Submitted to
Michigan State University
in partial fulfillment of the requirements
for the degree of

MASTER OF SCIENCE

Department of Electrical and Computer Engineering

2004

ABSTRACT

A PERIODIC LAYERED MEDIUM GREEN'S FUNCTION

By

Christopher P. Trampel

In this thesis, we derive a periodic Green's function for dipoles radiating inside a layered medium. In order to do so, we proceed as follows: first the spatial Green's function for a dipole inside a layer is derived in terms of Hertz potentials. Next, it is shown that this periodic Green's function can be calculated in the spectral domain provided that the Fourier integrals do not have poles on the real axis. The derived expressions indicate that this spectral sum is rapidly converging for most source-observation pairs. However, they are not so for the source and observation pair lying on either the top or bottom interfaces. To overcome this, a Kummer's transformation is proposed. We validate our Green's function via reduction to a canonical half-space problem. The periodic layered medium Green's function is validated numerically by comparison with analytical data for reflection and transmission from a single layer.

Copyright by $\label{eq:Christopher Paul Trampel}$ 2004

ACKNOWLEDGEMENTS

I would like to thank first and foremost my wife Mary for supporting me through the rigors of graduate school with her customary grace and empathy. Thanks also to my parents Christine and Darrell for their love and encouragement. I am also indebted to Dr. Shanker Balasubramaniam, Dr. Gregory Kobidze, Dr. Edward Rothwell, Dr. Dennis Nyquist, and Dr. Leo Kempel for their guidance during the writing of this thesis.

TABLE OF CONTENTS

LIST (OF FIGURES	vii
NOME	ENCLATURE	viii
СНАР	TER 1 INTRODUCTION	1
1.1	Plasmons	1
1.2	Numerical modelling of plasmons	1
1.3	Periodic layered medium Green's function	2
1.4	Organization	2
СНАР	TER 2 PERIODIC LAYERED MEDIUM GREEN'S FUNC-	
TIC	ON	4
2.1	Motivation	4
2.2	Problem Definition	5
	2.2.1 Tangential components	8
	2.2.2 Normal component	10
	2.2.3 Dyadic Green's function	11
2.3	Derivation of spectral series for general periodic Green's function	13
2.4	Kummer's Transformation	16
2.5	Surface Waves	19
СНАР	TER 3 RESULTS	21
3.1	Analytical validation of dyadic Green's function	21
	3.1.1 The Gxx and Gyy components	21
	3.1.2 The Gzx and Gzy components	22
	3.1.3 The Gzz component	24
3.2	Numerical validation of dyadic Green's function	24
СНАР	TER 4 CONCLUSION	28
APPE	NDIX A Components of dyadic Green's function	20

BIBLIOGRAPHY																																,	31
---------------------	--	--	--	--	--	--	--	--	--	--	--	--	--	--	--	--	--	--	--	--	--	--	--	--	--	--	--	--	--	--	--	---	----

LIST OF FIGURES

2.1	Layered medium formulation
2.2	A current element embedded in a single layer
3.1	(a) Transmission from 20 nm slab of $\epsilon_r = 4$ as a function of
	wavelength; (b) Transmission from 40 nm slab of $\epsilon_r = 4$ as a
	function of wavelength
3.2	Transmission from 20 nm slab of $\epsilon_r = 4$ as a function of angle 2

NOMENCLATURE

Lower case

 ϵ_n permittivity in layer n (s² · C² · kg⁻¹ · m⁻³)

 ϵ_0 permittivity in free space $(s^2 \cdot C^2 \cdot kg^{-1} \cdot m^{-3})$

 μ_0 permeability of free space (H · m⁻¹)

 ω temporal frequency (radians · s⁻¹)

Upper case

N unknowns

 $\mathbf{E}(\mathbf{r})$ electric field intensity $(\mathbf{V} \cdot \mathbf{m}^{-1})$

 $\mathbf{D}(\mathbf{r})$ electric flux density $(\mathbf{C} \cdot \mathbf{m}^{-2})$

 $\mathbf{H}(\mathbf{r})$ magnetic field intensity $(\mathbf{A} \cdot \mathbf{m}^{-1})$

Acronyms

EM electromagnetic

DE Differential Equation

IE Integral Equation

FDTD Finite Difference Time Domain

FMM Fast Multipole Method

AIM Adaptive Integral Method

CHAPTER 1 INTRODUCTION

1.1 Plasmons

Periodically structured dielectrics support waves bound to the surface of the object upon plane wave illumination. Specifically, dielectrics with negative real permittivity support charge density oscillations known as surface plasmons. The coupling between a surface wave and charge density oscillation is the so-called surface plasmon polariton.

Research into nano-plasmon optics is growing into a rich research field, with far reaching implications. Surface plasmon resonance interferometry techniques have yielded sensors for biological media [1]. Specifically, plasmonic sensors have been applied to the study of DNA [2]. Plasmons may also have application in quasi-planar lightwave circuits.

Plasmons have been studied extensively from a theoretical perspective. The dispersion relation for SPPs has been derived for a periodic array of scatterers at the interface between two infinite media [3], and the resulting dispersion curves show strong band gaps. Even more interesting optical properties of SPPs have been observed experimentally. Metal films perforated by periodically distributed holes exhibit stronger transmission than that predicted by geometrical optics [4]. These transmission peaks occur at the same frequencies as SPP modes. The mechanism of this enhanced transmission has been well studied and is related to the excitation of surface plasmons on both interfaces [5]. Coupling in this so-called surface plasmon polariton (SPP) molecule funnels energy from one interface to the other.

1.2 Numerical modelling of plasmons

Full wave analysis is necessary for study of plasmons supported by arbitrarily shaped geometries. However, the large negative real permittivity of metals at optical frequencies necessitates dense discretization in order to capture the wave physics. Since the holes occupy only 5% of the volume of a typical thin film, a sizeable region must be meshed.

We seek an integral equation scheme that will allow us to mesh only the hole region.

1.3 Periodic layered medium Green's function

To that end, we introduce the periodic Green's function for planarly layered media. The layered medium Green's function for a single arbitrarily oriented current element is well known. The electric dyadic Green's function for planarly layered media can be found in Chew [6]. The layered medium Green's function was derived in terms of potentials for planar media by Michalski et al. [7]. Both Chew and Michalski express the Green's function in the spatial domain in terms of inverse Fourier transforms. The spatial periodic Green's function is an infinite sum over a two-dimensional lattice of the Green's function for a single current element. However, any lattice sum may be computed in the spectral domain [8]. Pozar et al. derived a periodic Green's function for a current element above a grounded dielectric layer via spectral techniques [9].

In this thesis, we derive a spectral periodic Green's function for current elements radiating inside a layered medium. Our Green's function differs from Pozar's in that our current elements reside *inside* a layer backed by a dielectric, while his lie on top of a grounded dielectric slab. A new derivation of the Green's function for a current element inside a single layer is presented. We show how a spectral periodic Green's function may be obtained for an arbitrary spatial lattice sum. The resulting spectral layered medium periodic Green's exhibits exponential convergence for most source-observation pairs. However, the convergence is extremely slow when both the source and observation point lie on the same interface. We propose a technique to improve convergence for this case based on a Kummer's transformation [10].

1.4 Organization

The remainder of the thesis is organized as follows. Chapter 2 begins with the volume integral formulation for EM scattering from homogeneous dielectric bodies. This chapter includes a new derivation of the Green's function for a current element inside a single

layer, a derivation of the spectral series periodic Green's function for an arbitrary lattice sum, and the Kummer's transformation acceleration technique. A derivation of the dispersion relationship for surface waves supported by a single dielectric layer concludes the chapter. Chapter 3 details the analytical and numerical validation of the layered medium Green's function. Chapter 4 summarizes our conclusions and future work.

CHAPTER 2 PERIODIC LAYERED MEDIUM GREEN'S FUNCTION

2.1 Motivation

We begin by discussing the geometry in Figure 2.1. Consider a volume Ω bounded

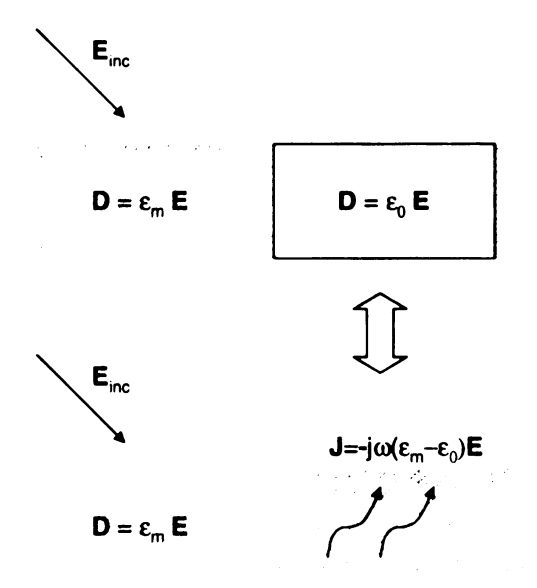


Figure 2.1 Layered medium formulation

by a surface $\partial\Omega$ that is embedded in a slab of permittivity ε_n ; either side of this slab are dielectric regions whose permittivity is denoted by ε_{n-1} and ε_{n+1} . The permittivity of the volume Ω is ε_0 . A plane wave described by $\{\mathbf{E}^i(\mathbf{r}), \mathbf{H}^i(\mathbf{r})\}$ is incident upon the dielectric. At this point, one can use either a surface or a volume equivalence theorems; while we have both working codes, we have chosen the latter presentation. Volume equivalence theorem permits us to replace free space with background permittivity ε_n and introduce an equivalent current density $\mathbf{J}(\mathbf{r}) = -j\omega(\varepsilon_n - \varepsilon_0)\mathbf{E}(\mathbf{r})$ such that the same fields are produced everywhere. Then using the fact that the total field $\mathbf{E}(\mathbf{r})$ is a superposition of the incident field and the scattered field results in the desired integral

equation:

$$\mathbf{E}(\mathbf{r}) = \mathbf{E}^{i}(\mathbf{r}) - \mathcal{L}\{\mathbf{J}(\mathbf{r})\}$$
 (2.1)

where

$$\mathcal{L}\{\mathbf{X}(\mathbf{r})\} \doteq \{k_n^2 + \nabla \nabla \cdot\} \int_{\Omega} dv' \bar{\mathbf{G}}_p(\mathbf{r}, \mathbf{r}') \cdot \frac{\mathbf{X}(\mathbf{r}')}{j\omega \varepsilon_n}, \tag{2.2}$$

 $\bar{\mathbf{G}}_p(\mathbf{r}, \mathbf{r}')$ is the periodic dyadic Green's function for a current element radiating in layered media, and k_n is the wavenumber in medium n.

2.2 Problem Definition

The starting point for the derivation of the Green's function for periodically arranged unknowns is the layered medium Green's function that is very well known. However, we have derived our own based on Hertz potentials which reduces to that given in [7] with appropriate scaling [11].

Consider a current element inside a layered medium (Figure 2.2). The radiated

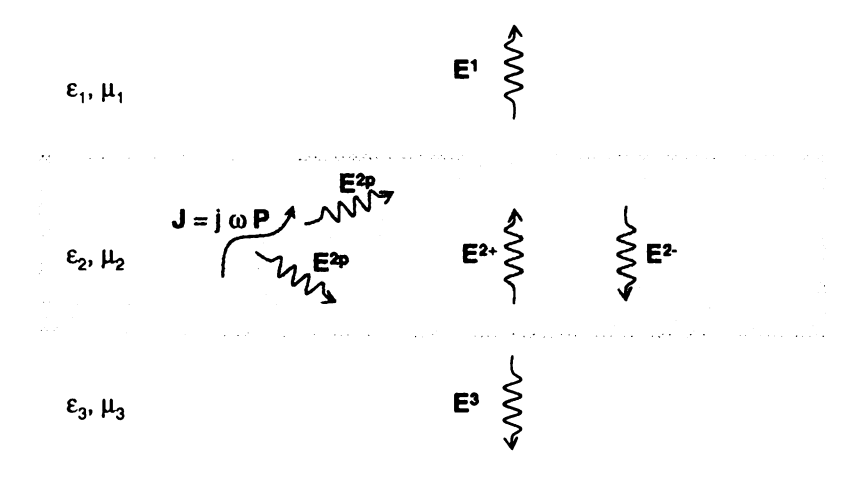


Figure 2.2 A current element embedded in a single layer

electric field is given by:

$$\mathbf{E}(\mathbf{r}) = \begin{cases} \mathbf{E}_{1}^{+}(\mathbf{r}), & z \geq h \\ \mathbf{E}_{2}^{p}(\mathbf{r}) + \mathbf{E}_{2}^{+}(\mathbf{r}) + \mathbf{E}_{2}^{-}(\mathbf{r}), & 0 \leq z \leq h \\ \mathbf{E}_{3}^{-}(\mathbf{r}), & z \leq 0 \end{cases}$$

$$(2.3)$$

The field in region 1 consists of a single up going wave. In region 2, the field has three constituents: a principal wave which acts as if it is in an unbounded medium (\mathbf{E}_2^p) , an up going wave (\mathbf{E}_2^+) , and a down going wave (\mathbf{E}_2^-) . A single down going wave represents the field in region 3.

We prefer to work with Hertz potentials as intermediate quantities. The electric field may be recovered from the Hertzian potential thus:

$$\mathbf{E}_{2}^{+}(\mathbf{r}) = k_{n}^{2} \pi_{2}^{+}(\mathbf{r}) + \nabla(\nabla \cdot \pi_{2}^{+}(\mathbf{r}))$$
(2.4)

$$\mathbf{E}_{2}^{-}(\mathbf{r}) = k_{n}^{2} \pi_{2}^{-}(\mathbf{r}) + \nabla(\nabla \cdot \pi_{2}^{-}(\mathbf{r}))$$

$$\tag{2.5}$$

$$\mathbf{E}_{2}^{p}(\mathbf{r}) = k_{n}^{2} \pi_{2}^{p}(\mathbf{r}) + \nabla(\nabla \cdot \pi_{2}^{p}(\mathbf{r}))$$
(2.6)

where n is the layer number, and k_n is the wavenumber in layer n. Each component of the Hertzian potential is expressed as an inverse transform:

$$\pi_{n\alpha}(\mathbf{r}) = \frac{1}{(2\pi)^2} \iint_{-\infty}^{\infty} W_{n\alpha}(\mathbf{k}) e^{j\mathbf{k}\cdot\boldsymbol{\rho}} e^{\pm jp(\mathbf{k})z} d^2k$$
 (2.7)

where $W_{n\alpha}(\mathbf{k})$ is an unknown amplitude spectrum, $\rho = x\hat{\mathbf{x}} + y\hat{\mathbf{y}}$, $\mathbf{k} = k_x\hat{\mathbf{x}} + k_y\hat{\mathbf{y}}$, $p(\mathbf{k}) = \sqrt{k_n^2 - (k_x^2 + k_y^2)}$, and k_x and k_y are the transform variables with respect to x and y. The sign before $p(\mathbf{k})$ determines the direction of propagation in the z direction: a positive sign indicates a down going wave while a negative sign indicates an up going wave. The up going and down going waves are homogeneous solutions to the Helmholtz

equation, while the principal wave is an inhomogeneous solution to the following:

$$\nabla^2 \pi_n^p(\mathbf{r}) + k_n^2 \pi_n^p(\mathbf{r}) = -\frac{\mathbf{J}(\mathbf{r})}{j\omega\epsilon_n}$$
(2.8)

where $\mathbf{J}(\mathbf{r})$ is the electric current. The principal wave $\pi_2^p(\mathbf{r})$ may be regarded as a particular solution to the above, while $\pi_2^+(\mathbf{r})$ and $\pi_2^-(\mathbf{r})$ are homogeneous solutions of the same.

Our derivation of the Green's function relies upon boundary conditions on the Hertz potential [11]. These boundary conditions are a direct consequence of continuity of tangential electric and magnetic field across an interface. The electric and magnetic fields are written in terms of Hertz potentials and the continuity of electric and magnetic fields across a boundary is imposed. A system of four equations results, one equation for each of the four tangential components of the electric and magnetic fields. When the components of the excitatory current **J** are considered independently, it is found that not all components of the Hertz potential are necessary to represent electric and magnetic fields that satisfy the boundary conditions. When the proper components of the Hertz potential are conjectured for the associated component of the current, the system of four equations imply boundary conditions on the components of the Hertz potential. The boundary conditions for the components of the Hertzian potential are summarized as follows [12]:

$$\pi_{n\alpha}(\mathbf{r}) = N_{n+1,n}^2 \pi_{(n+1)\alpha}(\mathbf{r}), \quad \alpha = x, y, z$$
(2.9)

$$\frac{\partial \pi_{n\alpha}(\mathbf{r})}{\partial z} = N_{n+1,n}^2 \frac{\partial \pi_{(n+1)\alpha}(\mathbf{r})}{\partial z}, \quad \alpha = x, y$$
 (2.10)

$$\left(\frac{\partial \pi_{nz}(\mathbf{r})}{\partial z} - \frac{\partial \pi_{(n+1)z}(\mathbf{r})}{\partial z}\right) = -(N_{n+1,n}^2 - 1)\left(\frac{\partial \pi_{(n+1)x}(\mathbf{r})}{\partial x} + \frac{\partial \pi_{(n+1)y}(\mathbf{r})}{\partial y}\right)$$
(2.11)

$$N_{n+1,n}^2 = \frac{\epsilon_{n+1}}{\epsilon_n} \tag{2.12}$$

where α is the component of the Hertzian potential (x,y,z).

2.2.1 Tangential components

The unknowns $W_{1\alpha}(\mathbf{k})$, $W_{2\alpha}^+(\mathbf{k})$, $W_{2\alpha}^-(\mathbf{k})$, $W_{3\alpha}(\mathbf{k})$ for the tangential components ($\alpha = x, y$) were found by applying boundary conditions 1 and 2 at interface 1-2 and 2-3. The first boundary condition at interface 1-2 leads to:

$$\pi_{1\alpha}(x,y,h) = N_{21}^2 \pi_{2\alpha}(x,y,h) \tag{2.13}$$

$$\pi_{1\alpha}(x,y,h) = N_{21}^{2} \{ \pi_{2\alpha}^{p}(x,y,h) + \pi_{2\alpha}^{+}(x,y,h) + \pi_{2\alpha}^{-}(x,y,h) \}$$
 (2.14)

Next, we substitute for the potentials in terms of inverse transforms:

$$\frac{1}{(2\pi)^2} \int_{-\infty}^{+\infty} d^2k W_{1\alpha}(\mathbf{k}) e^{j\mathbf{k}\cdot\rho} e^{-jp_1(\mathbf{k})h} =$$

$$N_{21}^2 \frac{1}{(2\pi)^2} \int_{-\infty}^{+\infty} d^2k \left\{ \frac{e^{j\mathbf{k}\cdot\rho}}{2\epsilon_2 p_2(\mathbf{k})} e^{-jp_2(\mathbf{k})h} + W_{2\alpha}^+(\mathbf{k}) e^{j\mathbf{k}\cdot\rho} e^{-jp_2(\mathbf{k})h} + W_{2\alpha}^-(\mathbf{k}) e^{j\mathbf{k}\cdot\rho} e^{jp_2(\mathbf{k})h} \right\}$$
(2.15)

$$\int_{-\infty}^{+\infty} d^2k \left[W_{1\alpha}(\mathbf{k}) e^{-jp_1(\mathbf{k})h} - N_{21}^2 \left\{ \frac{e^{-jp_2(\mathbf{k})h}}{2\epsilon_2 p_2(\mathbf{k})} + W_{2\alpha}^+(\mathbf{k}) e^{-jp_2(\mathbf{k})h} + W_{2\alpha}^-(\mathbf{k}) e^{jp_2(\mathbf{k})h} \right\} \right] e^{j\mathbf{k}\cdot\rho} = 0$$

$$(2.16)$$

Invoking the Fourier transform theorem:

$$W_{1\alpha}(\mathbf{k})e^{-jp_1(\mathbf{k})h} - N_{21}^2 \left\{ \frac{e^{-jp_2(\mathbf{k})h}}{2\epsilon_2 p_2(\mathbf{k})} + W_{2\alpha}^+(\mathbf{k})e^{-jp_2(\mathbf{k})h} + W_{2\alpha}^-(\mathbf{k})e^{jp_2(\mathbf{k})h} \right\} = 0 \qquad (2.17)$$

The above represents the first of four equations in the four unknowns $W_{1\alpha}(\mathbf{k})$, $W_{2\alpha}^+(\mathbf{k})$, $W_{2\alpha}^-(\mathbf{k})$, $W_{3\alpha}^-(\mathbf{k})$. The second boundary condition enforced at interface 1-2 yields:

$$\frac{\partial \pi_{1\alpha}(x,y,h)}{\partial z} = N_{21}^2 \frac{\partial \pi_{2\alpha}(x,y,h)}{\partial z} \frac{\partial \pi_{1\alpha}(x,y,h)}{\partial z} = N_{21}^2 \frac{\partial}{\partial z} \{\pi_{2\alpha}^p(x,y,h) + \pi_{2\alpha}^+(x,y,h) + \pi_{2\alpha}^-(x,y,h)\}$$
(2.18)

The first boundary condition applied at interface 2-3 yields:

$$\pi_{2\alpha}(x,y,0) = N_{32}^2 \pi_{3\alpha}(x,y,0) \tag{2.19}$$

$$\pi_{2\alpha}^{p}(x,y,0) + \pi_{2\alpha}^{+}(x,y,0) + \pi_{2\alpha}^{-}(x,y,0) = N_{32}^{2}\pi_{3\alpha}(x,y,0)$$
(2.20)

The second boundary condition enforced at interface 2-3 yields:

$$\frac{\partial \pi_{2\alpha}(x,y,0)}{\partial z} = N_{32}^2 \frac{\partial \pi_{3\alpha}(x,y,0)}{\partial z}$$
 (2.21)

$$\frac{\partial}{\partial z} \{ \pi_{2\alpha}^{p}(x,y,0) + \pi_{2\alpha}^{+}(x,y,0) + \pi_{2\alpha}^{-}(x,y,0) \} = N_{32}^{2} \frac{\partial \pi_{3\alpha}(x,y,0)}{\partial z}$$
 (2.22)

The final equations (2.23) are derived in a manner completely analogous to (2.17) by substituting for the potentials as transforms and using the Fourier transform theorem. For brevity, we summarize the equations resulting from imposing boundary conditions at both interfaces in matrix form:

$$\begin{bmatrix} e^{-jp_{1}(\mathbf{k})h} & -N_{21}^{2}e^{-jp_{2}(\mathbf{k})h} & -N_{21}^{2}e^{jp_{2}(\mathbf{k})h} & 0\\ e^{-jp_{1}(\mathbf{k})h} & -N_{21}^{2}\frac{p_{2}(\mathbf{k})}{p_{1}(\mathbf{k})}e^{-jp_{2}(\mathbf{k})h} & N_{21}^{2}\frac{p_{2}(\mathbf{k})}{p_{1}(\mathbf{k})}e^{jp_{2}(\mathbf{k})h} & 0\\ 0 & -1 & -1 & N_{32}^{2}\\ 0 & \frac{p_{2}(\mathbf{k})}{p_{3}(\mathbf{k})} & -\frac{p_{2}(\mathbf{k})}{p_{3}(\mathbf{k})} & N_{32}^{2} \end{bmatrix} \begin{bmatrix} W_{1\alpha}(\mathbf{k}) \\ W_{2\alpha}^{+}(\mathbf{k}) \\ W_{2\alpha}^{-}(\mathbf{k}) \\ W_{3\alpha}(\mathbf{k}) \end{bmatrix} = \begin{bmatrix} N_{21}^{2}V_{2\alpha}^{12}(\mathbf{k}) \\ N_{21}^{2}\frac{p_{2}(\mathbf{k})}{p_{1}(\mathbf{k})}V_{2\alpha}^{12}(\mathbf{k}) \\ V_{2\alpha}^{23}(\mathbf{k}) \\ W_{3\alpha}(\mathbf{k}) \end{bmatrix}$$

$$(2.23)$$

For notational simplicity we introduce:

$$V_{2\alpha}^{12}(\mathbf{k}) = \frac{e^{-jp_2(\mathbf{k})h}}{2\epsilon_2 p_2(\mathbf{k})}$$
 (2.24)

$$V_{2\alpha}^{23}(\mathbf{k}) = \frac{1}{2\epsilon_2 p_2(\mathbf{k})} \tag{2.25}$$

2.2.2 Normal component

The unknowns $W_{1z}(\mathbf{k})$, $W_{2z}^+(\mathbf{k})$, $W_{2z}^-(\mathbf{k})$, $W_{3z}(\mathbf{k})$ for the normal component were found by applying boundary conditions 1 and 3 at interface 1-2 and 2-3. The first boundary condition enforced at interface 1-2 leads to:

$$\pi_{1z}(x,y,h) = N_{21}^2 \pi_{2z}(x,y,h) \pi_{1z}(x,y,h) =$$

$$N_{21}^2 \{ \pi_{2z}^p(x,y,h) + \pi_{2z}^+(x,y,h) + \pi_{2z}^-(x,y,h) \}$$
(2.26)

The third boundary condition imposed at interface 1-2 gives:

$$\frac{\partial \pi_{1z}(x,y,h)}{\partial z} - \frac{\partial \pi_{2z}(x,y,h)}{\partial z} = -(N_{21}^2 - 1)(\frac{\partial \pi_{2x}(x,y,h)}{\partial x} + \frac{\partial \pi_{2y}(x,y,h)}{\partial y}) \qquad (2.27)$$

$$\frac{\partial \pi_{1z}(x,y,h)}{\partial z} - \frac{\partial}{\partial z} \left[\pi_{2z}^{p}(x,y,h) + \pi_{2z}^{+}(x,y,h) + \pi_{2z}^{-}(x,y,h) \right] =
- (N_{21}^{2} - 1) \left\{ \frac{\partial}{\partial x} \left[\pi_{2x}^{p}(x,y,h) + \pi_{2x}^{+}(x,y,h) + \pi_{2x}^{-}(x,y,h) \right] \right.
+ \frac{\partial}{\partial y} \left[\pi_{2y}^{p}(x,y,h) + \pi_{2y}^{+}(x,y,h) + \pi_{2y}^{-}(x,y,h) \right] \right\}$$
(2.28)

The first boundary condition enforced at interface 2-3 leads to:

$$\pi_{2z}(x,y,0) = N_{32}^2 \pi_{3z}(x,y,0) \pi_{2z}^p(x,y,0) + \pi_{2z}^+(x,y,0) + \pi_{2z}^-(x,y,0) = N_{32}^2 \pi_{3z}(x,y,0)$$
(2.29)

The third boundary condition imposed at interface 2-3 gives:

$$\frac{\partial \pi_{2z}(x,y,0)}{\partial z} - \frac{\partial \pi_{3z}(x,y,0)}{\partial z} = -(N_{32}^2 - 1)(\frac{\partial \pi_{3x}(x,y,0)}{\partial x} + \frac{\partial \pi_{3y}(x,y,0)}{\partial y})$$
(2.30)

$$\frac{\partial}{\partial z} \left[\pi_{2z}^{p}(x, y, 0) + \pi_{2z}^{+}(x, y, 0) + \pi_{2z}^{-}(x, y, 0) \right] - \frac{\partial \pi_{3z}(x, y, 0)}{\partial z} =
- (N_{32}^{2} - 1) \left\{ \frac{\partial}{\partial x} \left[\pi_{2x}^{p}(x, y, 0) + \pi_{2x}^{+}(x, y, 0) + \pi_{2x}^{-}(x, y, 0) \right] \right\}
+ \frac{\partial}{\partial y} \left[\pi_{2y}^{p}(x, y, 0) + \pi_{2y}^{+}(x, y, 0) + \pi_{2y}^{-}(x, y, 0) \right] \right\}$$
(2.31)

The final equations (2.32) are derived by substituting for the potentials as transforms and using the Fourier transform theorem. For brevity, we summarize the equations resulting from imposing boundary conditions at both interfaces in matrix form:

$$\begin{bmatrix} e^{-jp_{1}(\mathbf{k})h} & -N_{21}^{2}e^{-jp_{2}(\mathbf{k})h} & -N_{21}^{2}e^{jp_{2}(\mathbf{k})h} & 0\\ -e^{-jp_{1}(\mathbf{k})h} & \frac{p_{2}(\mathbf{k})}{p_{1}(\mathbf{k})}e^{-jp_{2}(\mathbf{k})h} & -\frac{p_{2}(\mathbf{k})}{p_{1}(\mathbf{k})}e^{jp_{2}(\mathbf{k})h} & 0\\ 0 & -1 & -1 & N_{32}^{2}\\ 0 & 1 & -1 & \frac{p_{3}(\mathbf{k})}{p_{2}(\mathbf{k})} \end{bmatrix} \begin{bmatrix} W_{1z}(\mathbf{k})\\ W_{2z}^{+}(\mathbf{k})\\ W_{2z}^{-}(\mathbf{k})\\ W_{3z}(\mathbf{k}) \end{bmatrix} = \begin{bmatrix} A\\ B\\ C\\ D \end{bmatrix}$$
(2.32)

where

$$\begin{bmatrix} A \\ B \\ C \\ D \end{bmatrix} = \begin{bmatrix} N_{21}^{2}V_{2z}^{12}(\mathbf{k}) \\ \left[-\frac{p_{2}(\mathbf{k})}{p_{1}(\mathbf{k})}V_{2z}^{12}(\mathbf{k}) - \frac{(N_{21}^{2}-1)}{p_{1}(\mathbf{k})} \left\{ k_{x}W_{2x}^{+}(\mathbf{k})e^{-jp_{2}(\mathbf{k})} + k_{y}W_{2y}^{+}(\mathbf{k})e^{-jp_{2}(\mathbf{k})} + k_{y}W_{2y}^{-}(\mathbf{k})e^{jp_{2}(\mathbf{k})} + k_{x}V_{2x}^{12}(\mathbf{k}) + k_{y}V_{2y}^{12}(\mathbf{k}) \right\} \right] \\ V_{2z}^{23}(\mathbf{k}) \\ V_{2z}^{23}(\mathbf{k}) + \frac{(N_{3z}^{2}-1)}{p_{2}(\mathbf{k})} \left\{ k_{x}W_{3x}(\mathbf{k}) + k_{y}W_{3y}(\mathbf{k}) \right\} \end{bmatrix}$$
(2.33)

2.2.3 Dyadic Green's function

After solving these two systems, the total Hertzian potential for region two may be expressed as a superposition of three waves.

$$\pi_{2\alpha}(\mathbf{r}) = \pi_{2\alpha}^{p}(\mathbf{r}) + \pi_{2\alpha}^{+}(\mathbf{r}) + \pi_{2\alpha}^{-}(\mathbf{r})$$
(2.34)

$$\pi_{2\alpha}(\mathbf{r}) = \frac{1}{(2\pi)^2} \int_{-\infty}^{+\infty} d^2k \left\{ \frac{e^{j\mathbf{k}\cdot\rho}}{2\epsilon_2 p_2(\mathbf{k})} e^{-jp_2(\mathbf{k})z} + W_{2\alpha}^+(\mathbf{k}) e^{j\mathbf{k}\cdot\rho} e^{-jp_2(\mathbf{k})z} + W_{2\alpha}^-(\mathbf{k}) e^{j\mathbf{k}\cdot\rho} e^{jp_2(\mathbf{k})z} \right\}$$

(2.35)

$$\pi_{2\alpha}(\mathbf{r}) = \frac{1}{(2\pi)^2} \int_{-\infty}^{+\infty} d^2k \left\{ \frac{e^{j\mathbf{k}\cdot\boldsymbol{\rho}}}{2\epsilon_2 p_2(\mathbf{k})} e^{-jp_2(\mathbf{k})z} \right.$$

$$+ \frac{R_{21}^t(\mathbf{k}) R_{23}^t(\mathbf{k}) e^{-jp_2(\mathbf{k})} V_{2\alpha}^{12}(\mathbf{k}) + R_{23}^t(\mathbf{k}) V_{2\alpha}^{23}(\mathbf{k})}{(1 + R_{12}^t(\mathbf{k}) R_{23}^t(\mathbf{k}) e^{-j2p_2(\mathbf{k})h})} e^{j\mathbf{k}\cdot\boldsymbol{\rho}} e^{-jp_2(\mathbf{k})z}$$

$$+ \frac{R_{21}^t(\mathbf{k}) e^{-jp_2(\mathbf{k})} V_{2\alpha}^{12}(\mathbf{k}) + R_{21}^t(\mathbf{k}) R_{23}^t(\mathbf{k}) e^{-j2p_2(\mathbf{k})} V_{2\alpha}^{23}(\mathbf{k})}{(1 - R_{21}^t(\mathbf{k}) R_{23}^t(\mathbf{k}) e^{-j2p_2(\mathbf{k})h})} e^{j\mathbf{k}\cdot\boldsymbol{\rho}} e^{jp_2(\mathbf{k})z} \right\}$$

$$(2.36)$$

where

$$R_{mn}^{t}(\mathbf{k}) = \frac{p_{m}(\mathbf{k}) - p_{n}(\mathbf{k})}{p_{m}(\mathbf{k}) + p_{n}(\mathbf{k})}$$
(2.37)

Substituting for $V_{2\alpha}^{12}(\mathbf{k})$ and $V_{2\alpha}^{23}(\mathbf{k})$:

$$\pi_{2\alpha}(\mathbf{r}) = \frac{1}{(2\pi)^2} \int_{-\infty}^{+\infty} d^2k \left\{ \frac{e^{j\mathbf{k}\cdot\boldsymbol{\rho}}}{2\epsilon_2 p_2(\mathbf{k})} e^{-jp_2(\mathbf{k})z} \right.$$

$$+ \left\{ \frac{R_{21}^t(\mathbf{k}) R_{23}^t(\mathbf{k}) e^{-jp_2(\mathbf{k})h}}{2\epsilon_2 p_2(\mathbf{k}) (1 - R_{21}^t(\mathbf{k}) R_{23}^t(\mathbf{k}) e^{-j2p_2(\mathbf{k})h})} \right.$$

$$+ \frac{R_{23}^t(\mathbf{k})}{2\epsilon_2 p_2(\mathbf{k}) (1 - R_{21}^t(\mathbf{k}) R_{23}^t(\mathbf{k}) e^{-j2p_2(\mathbf{k})h})} \right\} e^{j\mathbf{k}\cdot\boldsymbol{\rho}} e^{-jp_2(\mathbf{k})z}$$

$$+ \left\{ \frac{R_{21}^t(\mathbf{k}) e^{-j2p_2(\mathbf{k})}}{2\epsilon_2 p_2(\mathbf{k}) (1 - R_{21}^t(\mathbf{k}) R_{23}^t(\mathbf{k}) e^{-j2p_2(\mathbf{k})h})} \right.$$

$$+ \frac{R_{21}^t(\mathbf{k}) R_{23}^t(\mathbf{k}) e^{-j2p_2(\mathbf{k})}}{2\epsilon_2 p_2(\mathbf{k}) (1 - R_{21}^t(\mathbf{k}) R_{23}^t(\mathbf{k}) e^{-j2p_2(\mathbf{k})h})} \right\} e^{j\mathbf{k}\cdot\boldsymbol{\rho}} e^{jp_2(\mathbf{k})z} \right\}$$

$$\pi_{2\alpha}(\mathbf{r}) = \frac{1}{(2\pi)^{2}} \int_{-\infty}^{+\infty} d^{2}k e^{j\mathbf{k}\cdot\rho} \left\{ \frac{e^{-jp_{2}(\mathbf{k})z}}{2\epsilon_{2}p_{2}(\mathbf{k})} + \frac{R_{21}^{t}(\mathbf{k})R_{23}^{t}(\mathbf{k})e^{-j2p_{2}(\mathbf{k})h}e^{-jp_{2}(\mathbf{k})z} + R_{23}^{t}(\mathbf{k})e^{-jp_{2}(\mathbf{k})z}}{2\epsilon_{2}p_{2}(\mathbf{k})(1 - R_{21}^{t}(\mathbf{k})R_{23}^{t}(\mathbf{k})e^{j\mathbf{k}\cdot\rho})} + \frac{R_{21}^{t}(\mathbf{k})e^{-j2p_{2}(\mathbf{k})}e^{jp_{2}(\mathbf{k})z} + R_{21}^{t}(\mathbf{k})R_{23}^{t}(\mathbf{k})e^{-j2p_{2}(\mathbf{k})}e^{jp_{2}(\mathbf{k})z}}{2\epsilon_{2}p_{2}(\mathbf{k})(1 - R_{21}^{t}(\mathbf{k})R_{23}^{t}(\mathbf{k})e^{-j2p_{2}(\mathbf{k})h})} \right\}$$

$$(2.39)$$

The above implies that the Green's function is:

$$G_{2\alpha}(\mathbf{R}) = \frac{1}{(2\pi)^2} \int_{-\infty}^{+\infty} d^2k \left\{ \frac{e^{-jp_2(\mathbf{k})|z-z'|}}{2\epsilon_2 p_2(\mathbf{k})} + \frac{R_{21}^t(\mathbf{k}) R_{23}^t(\mathbf{k}) e^{-j2p_2(\mathbf{k})h} e^{-jp_2(\mathbf{k})(z-z')} + R_{23}^t(\mathbf{k}) e^{-jp_2(\mathbf{k})(z+z')}}{2\epsilon_2 p_2(\mathbf{k}) (1 - R_{21}^t(\mathbf{k}) R_{23}^t(\mathbf{k}) e^{j\mathbf{k}\cdot\rho})} + \frac{R_{21}^t(\mathbf{k}) e^{-j2p_2(\mathbf{k})} e^{jp_2(\mathbf{k})(z+z')} + R_{21}^t(\mathbf{k}) R_{23}^t(\mathbf{k}) e^{-j2p_2(\mathbf{k})} e^{jp_2(\mathbf{k})(z-z')}}{2\epsilon_2 p_2(\mathbf{k}) (1 - R_{21}^t(\mathbf{k}) R_{23}^t(\mathbf{k}) e^{-j2p_2(\mathbf{k})h})} \right\} e^{j\mathbf{k}\cdot(\rho-\rho')}$$

The normal components of the dyadic Green's function are derived in a manner analogous to that used above. The total dyadic Green's function can be written in the spectral domain as:

$$\bar{\mathbf{G}}(\mathbf{k}, \mathbf{R}) = G^p(\mathbf{k}, \mathbf{R})\bar{\mathbf{I}} + \bar{\mathbf{G}}^r(\mathbf{k}, \mathbf{R})$$
(2.41)

where
$$G^p(\mathbf{k}, \mathbf{R}) = \frac{e^{-jk_2R}}{4\pi R}$$
, $R = \sqrt{(x-x')^2 + (y-y')^2 + (z-z')^2}$, and

$$\bar{\mathbf{G}}^{r}(\mathbf{k}, \mathbf{R}) = R_{xx}(\mathbf{k}, \mathbf{R})\hat{\mathbf{x}}\hat{\mathbf{x}} + R_{yy}(\mathbf{k}, \mathbf{R})\hat{\mathbf{y}}\hat{\mathbf{y}}
+ R_{zx}(\mathbf{k}, \mathbf{R})\hat{\mathbf{z}}\hat{\mathbf{x}} + R_{zy}(\mathbf{k}, \mathbf{R})\hat{\mathbf{z}}\hat{\mathbf{y}} + R_{zz}(\mathbf{k}, \mathbf{R})\hat{\mathbf{z}}\hat{\mathbf{z}}$$
(2.42)

(See Appendix for coefficients $R_{\alpha\beta}({\bf k},{\bf R}), \alpha=x,y,z,\beta=x,y,z.$)

2.3 Derivation of spectral series for general periodic Green's function

Electromagnetic (EM) scattering from a periodic structure can be captured via analysis of a single mother cell by employing a periodic Green's function. Linearity of our integral equations allows us to represent the field radiated by current elements distributed uniformly along the lattice as a superposition of isolated current elements distributed over the entire lattice. Thus the periodic Green's function is given by:

$$\bar{\mathbf{G}}_{p}(\mathbf{R}) = \sum_{u=-\infty}^{\infty} \sum_{v=-\infty}^{\infty} \bar{\mathbf{G}}(x - x' - uD_{x}, y - y' - vD_{y}, z - z') e^{-ju\beta_{x}D_{x}} e^{-jv\beta_{y}D_{y}}$$
 (2.43)

where $\bar{\mathbf{G}}(\mathbf{R})$ is the dyadic layered medium Green's function, D_x and D_y is the lattice spacing in the x and y directions, and β_x and β_y are the x and y components of the wave vector of the incident field. In most situations, the above converges slowly in the spatial domain. We seek an alternative form of the periodic Green's function with exponential convergence. To that end, the previous equation may be rewritten as follows:

$$\bar{\mathbf{G}}_{p}(\mathbf{R}) = \bar{\mathbf{G}}(\mathbf{R}) * \sum_{u=-\infty}^{\infty} \sum_{v=-\infty}^{\infty} \delta(x - x' - uD_{x}, y - y' - vD_{y}) e^{-ju\beta_{x}D_{x}} e^{-jv\beta_{y}D_{y}}$$
(2.44)

where * denotes convolution. Next we Fourier transform with respect to both x and y and invoke the multiplication property of the Fourier transform:

$$\tilde{\bar{\mathbf{G}}}_{p}(k_{x}, k_{y}, z - z') = \sum_{u = -\infty}^{\infty} \sum_{v = -\infty}^{\infty} \tilde{\bar{\mathbf{G}}}(k_{x}, k_{y}, z - z') \delta(k_{x} - \frac{u}{D_{x}} - \frac{\beta_{x}}{2\pi}, k_{y} - \frac{v}{D_{y}} - \frac{\beta_{y}}{2\pi})$$
(2.45)

where $\tilde{\mathbf{G}}(k_x,k_y,z-z')$ is the Fourier transform of the Green's function. Next, we take the inverse Fourier Transform to restore the spatial representation $\bar{\mathbf{G}}_p(\mathbf{R})$:

$$\bar{\mathbf{G}}_{p}(\mathbf{R}) = \sum_{u=-\infty}^{\infty} \sum_{v=-\infty}^{\infty} \frac{1}{(2\pi)^{2}} \iint_{-\infty}^{\infty} dk_{x} dk_{y} \tilde{\bar{\mathbf{G}}}(k_{x}, k_{y}, z - z') \cdot \delta(k_{x} - \frac{u}{D_{x}} - \frac{\beta_{x}}{2\pi}, k_{y} - \frac{v}{D_{y}} - \frac{\beta_{y}}{2\pi}) e^{jk_{x}(x-x')} e^{jk_{y}(y-y')}$$
(2.46)

Finally, we invoke the sampling property of the delta function:

$$\bar{\mathbf{G}}_{p}(\mathbf{R}) = \sum_{u=-\infty}^{\infty} \sum_{v=-\infty}^{\infty} \frac{1}{(2\pi)^{2}} \tilde{\mathbf{G}}(\frac{u}{D_{x}} + \frac{\beta_{x}}{2\pi}, \frac{v}{D_{y}} + \frac{\beta_{y}}{2\pi}, z - z') \cdot \exp(j(\frac{u}{D_{x}} + \frac{\beta_{x}}{2\pi})(x - x')) \exp(j(\frac{v}{D_{y}} + \frac{\beta_{y}}{2\pi})(y - y'))$$
(2.47)

This spectral series periodic Green's function is a superposition of the Fourier transform of the isolated Green's function sampled at appropriate intervals. Observe that the periodic Green's function is computed in the spectral domain. One cautionary remark must be made. Spectral domain summation is valid only if the Green's function has no poles along the real axis. Fortunately, our models for the metal contain a small loss which raises these poles off the real axis. With these caveats the Green's function may be computed thus:

$$\bar{\mathbf{G}}_{p}(\mathbf{R}) = \sum_{u=-\infty}^{\infty} \sum_{v=-\infty}^{\infty} \bar{\mathbf{G}}^{P}(x - x' - uD_{x}, y - y' - vD_{y}, z - z') \exp(-ju\beta_{x}D_{x} - jv\beta_{y}D_{y})
+ \sum_{u=-\infty}^{\infty} \sum_{v=-\infty}^{\infty} \bar{\mathbf{G}}^{R}(x - x' - uD_{x}, y - y' - vD_{y}, z - z') \exp(-ju\beta_{x}D_{x} - jv\beta_{y}D_{y})$$
(2.48)

where D_x and D_y is the lattice spacing in the x and y directions, β_x and β_y are the x and y components of the wave vector of the incident field, and $\mathbf{\bar{G}}^P$ and $\mathbf{\bar{G}}^R$ are the same as in (2.41). The sum over the principal wave is computed using an Ewald series for on-plane sources and observations and a spectral series for the off-plane cases. The phase accumulated as a result of reflections facilitates spectral domain summation of $\mathbf{\bar{G}}^R(\mathbf{R})$.

$$\bar{\mathbf{G}}_{p}^{R}(\mathbf{R}) = \sum_{u=-\infty}^{\infty} \sum_{v=-\infty}^{\infty} \frac{1}{(2\pi)^{2}} \tilde{\mathbf{G}}^{R}(\frac{2\pi u}{D_{x}} + \beta_{x}, \frac{2\pi v}{D_{y}} + \beta_{y}, z - z') \cdot \exp(j(\frac{2\pi u}{D_{x}} + \beta_{x})(x - x')) \exp(j(\frac{2\pi v}{D_{y}} + \beta_{y})(y - y'))$$
(2.49)

where $\tilde{\bar{\mathbf{G}}}^R(k_x,k_y,z-z')$ is the Fourier transform of $\bar{\mathbf{G}}^R(\mathbf{R})$.

2.4 Kummer's Transformation

Next we consider the efficiency of the spectral domain periodic Green's function. Our goal is exponential convergence for all source-observation pairs. Let us consider $R_{zz}(\mathbf{k}, \mathbf{R})$ term by term:

$$R_{zz}(\mathbf{k}, \mathbf{R}) = \frac{1}{2(2\pi)^{2} \epsilon_{2} p_{2}(\mathbf{k})} [R_{21}^{n}(\mathbf{k}) R_{23}^{n}(\mathbf{k}) e^{-j2p_{2}(\mathbf{k})h} e^{-jp_{2}(\mathbf{k})(z-z')}$$

$$+ R_{23}^{n}(\mathbf{k}) e^{-jp_{2}(\mathbf{k})(z+z')} + R_{21}^{n}(\mathbf{k}) e^{-j2p_{2}(\mathbf{k})h} e^{jp_{2}(\mathbf{k})(z+z')}$$

$$+ R_{21}^{n}(\mathbf{k}) R_{23}^{n}(\mathbf{k}) e^{-j2p_{2}(\mathbf{k})h} e^{jp_{2}(\mathbf{k})(z-z')}] \frac{e^{j\mathbf{k}\cdot(\rho-\rho')}}{1 - R_{21}^{n}(\mathbf{k}) R_{23}^{n}(\mathbf{k}) e^{-j2p_{2}(\mathbf{k})h}}$$

$$(2.50)$$

$$R_{ml}^{n}(\mathbf{k}) = \frac{N_{lm}^{2} p_{m}(\mathbf{k}) - p_{l}(\mathbf{k})}{N_{lm}^{2} p_{m}(\mathbf{k}) + p_{l}(\mathbf{k})}$$

$$(2.51)$$

The phase represented by the $e^{-jp_2(\mathbf{k})(z+z')}$ terms provide exponential convergence for source-observation pairs that are well separated in the z-direction. However, the summation is inefficient for source and and observation points which lie near the same interface. The two problem terms are:

$$R_{z21}(\mathbf{k}, \mathbf{R}) = \frac{1}{2(2\pi)^2 \epsilon_2 p_2(\mathbf{k})} R_{21}^n(\mathbf{k}) e^{-j2p_2(\mathbf{k})h} e^{jp_2(\mathbf{k})(z+z')} \frac{e^{j\mathbf{k}\cdot(\rho-\rho')}}{1 - R_{21}^n(\mathbf{k})R_{23}^n(\mathbf{k})e^{-j2p_2(\mathbf{k})h}}$$
(2.52)

$$R_{z23}(\mathbf{k}, \mathbf{R}) = \frac{1}{2(2\pi)^2 \epsilon_2 p_2(\mathbf{k})} R_{23}^n(\mathbf{k}) e^{-jp_2(\mathbf{k})(z+z')} \frac{e^{j\mathbf{k}\cdot(\rho-\rho')}}{1 - R_{21}^n(\mathbf{k}) R_{23}^n(\mathbf{k}) e^{-j2p_2(\mathbf{k})h}}$$
(2.53)

Consider the spectral summation of $R_{z12}(u, v)$:

$$\sum_{u=-\infty}^{+\infty} \sum_{v=-\infty}^{+\infty} R_{z21}(u,v) = \sum_{u=-\infty}^{+\infty} \sum_{v=-\infty}^{+\infty} \frac{1}{2(2\pi)^2 \epsilon_2 p_2(u,v)} R_{21}^n(u,v) \cdot \exp(-j2p_2(u,v)h + jp_2(u,v)(z+z')) \frac{\exp(j\mathbf{k} \cdot (\rho - \rho'))}{1 - R_{21}^n(u,v) R_{23}^n(u,v) \exp(-j2p_2(u,v)h)}$$
(2.54)

where $p_n(u,v) = \sqrt{k_n^2 - (k_{x0} + u \frac{2\pi}{D_x})^2 - (k_{y0} + v \frac{2\pi}{D_y})^2}$, D_x and D_y are the lattice spacing in the x and y directions, respectively. It is easy to see that when $(k_{x0} + u \frac{2\pi}{D_x})^2 + u \frac{2\pi}{D_x}$

 $(k_{y0}+v\frac{2\pi}{D_y})^2$ becomes larger than k_n^2 , $p_n(u,v)$ becomes a complex number. Choosing the negative root results in a quantity of the form $p_n(u,v)=-jL$ where L is a positive real number. Substituting into the phase term yields $e^{-jp_2(u,v)(z+z')}=e^{-L(z+z')}$ which is a decaying exponential. Thus source-observation pairs that lie above the bottom interface yield exponential convergence. While all components of the Green's function are adversely affected in this case, most still converge as $\mathcal{O}(\frac{1}{u^2})$ as $u \to \infty$. Consider the asymptotic behavior of a typical term from the G_{zx} component evaluated at z=z'=0:

$$R_{zx}^{t}(u,v) = \frac{1}{2(2\pi)^{2}\epsilon_{2}p_{2}(u,v)} \frac{N_{32}^{2} - 1}{p_{3}(u,v) + N_{32}^{2}p_{2}(u,v)} T_{23}^{t}(u,v)$$
(2.55)

We analyze the behavior of each term sequentially. Consider:

$$T_{23}^{t}(u,v) = \frac{2p_{2}(u,v)}{p_{2}(u,v) + p_{3}(u,v)} = \frac{2}{1 + \frac{p_{3}(u,v)}{p_{2}(u,v)}}$$
(2.56)

Now $\frac{p_3(u,v)}{p_2(u,v)} \to 1$ as $u,v \to \infty$. Thus $T^t_{23}(u,v) \to 1$. Without loss of generality we set u=v. Since $p_2(u) \to u$ as $u \to \infty$:

$$R_{zx}^{t}(u) \to \frac{1}{2\sqrt{2}(2\pi)^{2}\epsilon_{2}} \frac{N_{32}^{2} - 1}{1 + N_{32}^{2}} \frac{1}{u^{2}}$$
 (2.57)

Clearly this sum converges as $\mathcal{O}(\frac{1}{u^2})$.

The problem term is $R_{zz}(u,v)$ which converges as $\mathcal{O}(\frac{1}{u})$ for the on plane case. In the interest of brevity we support this claim for $R_{z21}(u,v)$ only:

$$R_{z21}(u,v) = \frac{1}{2(2\pi)^2 \epsilon_2 p_2(u,v)} R_{21}^n(u,v) \cdot \exp(-j2p_2(u,v)h + jp_2(u,v)(z+z')) \frac{\exp(j\mathbf{k} \cdot (\rho - \rho'))}{1 - R_{21}^n(u,v)R_{23}^n(u,v)\exp(-j2p_2(u,v)h)}$$
(2.58)

We begin with the asymptotic behavior of the reflection coefficients. To that end we

rewrite

$$R_{21}^{n}(u,v) = \frac{N_{12}^{2} \frac{p_{2}(u,v)}{p_{1}(u,v)} - 1}{N_{12}^{2} \frac{p_{2}(u,v)}{p_{1}(u,v)} + 1}$$
(2.59)

Observe that $\frac{p_2(u,v)}{p_1(u,v)} \to 1$ as $u,v \to \infty$. Also, the $e^{-j2p_2(u,v)h}$ term in the denominator rapidly decays to 0. Thus the asymptotic behavior of $R_{z21}(u,v)$ is:

$$R_{z21}(u,v) \to \frac{1}{2(2\pi)^2 \epsilon_2 p_2(u,v)} \frac{N_{12}^2 - 1}{N_{12}^2 + 1} e^{-j2p_2(u,v)h} e^{jp_2(u,v)(z+z')} e^{j\mathbf{k}\cdot(\rho-\rho')}$$
(2.60)

Setting z + z' = 2h (both source and observation points lie on the first interface) and u = v:

$$R_{z21}(u) \to \frac{N_{12}^2 - 1}{N_{12}^2 + 1} \frac{1}{2\sqrt{2}(2\pi)^2} \frac{e^{j\mathbf{k}\cdot(\rho - \rho')}}{p_2(u)} \to \frac{N_{12}^2 - 1}{N_{12}^2 + 1} \frac{1}{2\sqrt{2}(2\pi)^2} \frac{e^{j\mathbf{k}\cdot(\rho - \rho')}}{u}$$
(2.61)

Therefore, the sum to converges as $\mathcal{O}(\frac{1}{u})$. We accelerate the convergence by first observing that $R_{z12}(u,v)$ is simply a constant times the principal part of the Green's function.

$$R_{z21}(u,v) \to \frac{N_{12}^2 - 1}{N_{12}^2 + 1} G^P(u,v)$$
 (2.62)

We can exploit this term by term convergence towards the principal Green's function. In a Kummer's transformation, a series that can be summed quickly is added and subtracted to a slowly converging series. Here we simply add and subtract a scaled version of the principal Green's function. The summation over R_{z12} is broken into two parts, S_1 and S_2 .

$$\sum_{u=-\infty}^{+\infty} \sum_{v=-\infty}^{+\infty} R_{z21}(u,v) = \sum_{u=-\infty}^{+\infty} \sum_{v=-\infty}^{+\infty} S_1(u,v) + \sum_{u=-\infty}^{+\infty} \sum_{v=-\infty}^{+\infty} S_2(u,v)$$
 (2.63)

$$S_{1}(u,v) = \frac{1}{2(2\pi)^{2} \epsilon_{2} p_{2}(u,v)} R_{21}^{n}(u,v) e^{-j2p_{2}(u,v)h} e^{jp_{2}(u,v)(z+z')}.$$

$$\frac{e^{j\mathbf{k}\cdot(\rho-\rho')}}{1 - R_{21}^{n}(u,v)R_{23}^{n}(u,v)e^{-j2p_{2}(u,v)h}} - \frac{N_{12}^{2} - 1}{N_{12}^{2} + 1} G^{P}(u,v)$$
(2.64)

$$S_2(u,v) = \frac{N_{12}^2 - 1}{N_{12}^2 + 1} G^P(u,v)$$
(2.65)

Consider the summation of $S_1(u, v)$. As $u, v \to \infty$, the first term approaches the second and thus $S_1(u, v) \to 0$. The asymptotic behavior of the first term causes S_1 to converge rapidly. The summation of S_2 is evaluated by the usual spectral or Ewald series and therefore displays exponential convergence.

2.5 Surface Waves

Coupling between plasmons and surface waves is responsible for many of the interesting optical properties of thin films. Investigating the dispersion relationship for these bound waves will allow us to excite specific surface wave modes and provide further insight into the enhanced transmission phenomenon. For dielectrics with negative real epsilon, only the TM modes yield proper surface waves. The dispersion relationship for TM waves may be found by setting the denominator of the $R_{zz}(\mathbf{k}, R)$ term to zero:

$$1 - R_{21}^{n}(\mathbf{k})R_{23}^{n}(\mathbf{k})e^{-j2p_{2}(\mathbf{k})h} = 0$$
(2.66)

As a check on the above, we derive an equivalent expression from first principles. We begin our analysis be writing expressions for the field in each region.

$$H_{x}(y,z) = \begin{cases} C\exp(-qz - j\omega t + j\beta y), & z \ge h \\ \{A\cos(uz) + B\sin(uz)\}\exp(-j\omega t + j\beta y), & 0 \le z \le h \end{cases}$$

$$D\exp(vz - j\omega t + j\beta y), & z \le 0$$

$$(2.67)$$

Here, q, u, v are the spatial frequencies in region 1, 2, and 3 respectively and A, B, C and D are unknown amplitudes. Maxwell's equations provide an expression for E_y :

$$E_{y}(y,z) = -\frac{1}{j\omega\epsilon} \frac{\partial H_{x}(y,z)}{\partial z}$$
 (2.68)

Next, the we enforce continuity of the tangential electric and magnetic fields at both interfaces. The resulting system of equations may be written in matrix form thus:

$$\begin{bmatrix} \cos(uh) & \sin(uh) & -\exp(-qh) & 0 \\ -\frac{u}{\epsilon_2}\sin(uh) & \frac{u}{\epsilon_2}\cos(uh) & \frac{q}{\epsilon_1}\exp(-qh) & 0 \\ 1 & 0 & 0 & -1 \\ 0 & \frac{u}{\epsilon_2} & -\frac{v}{\epsilon_1} & 0 \end{bmatrix} \begin{bmatrix} A \\ B \\ C \\ D \end{bmatrix} = \begin{bmatrix} 0 \\ 0 \\ 0 \\ 0 \end{bmatrix}$$
(2.69)

Setting the determinant of this matrix to zero leads to the following implicit relationship between u, v, and q:

$$\frac{ve^{qh}}{\epsilon_2\epsilon_3} = \frac{u}{\epsilon_2^2}\sin(uh) - \frac{v}{\epsilon_1\epsilon_2}\cos(uh) \tag{2.70}$$

We seek a relationship between the spatial frequency, β , and temporal frequency, ω . To that end, we recognize that phase continuity requires that :

$$\beta^2 - q^2 = \omega^2 \mu_0 \epsilon_1 \tag{2.71}$$

$$\beta^2 + u^2 = \omega^2 \mu_0 \epsilon_2 \tag{2.72}$$

$$\beta^2 - v^2 = \omega^2 \mu_0 \epsilon_3 \tag{2.73}$$

Eliminating u, q and v:

$$\frac{\sqrt{\beta^2 - \omega^2 \mu_0 \epsilon_3} e^{\sqrt{\beta^2 - \omega^2 \mu_0 \epsilon_1} h}}{\frac{\epsilon_2 \epsilon_3}{\sqrt{\omega^2 \mu_0 \epsilon_2 - \beta^2}}} = \frac{1}{\sqrt{\omega^2 \mu_0 \epsilon_2 - \beta^2}} \sin(\sqrt{\omega^2 \mu_0 \epsilon_2 - \beta^2} h) - \frac{\sqrt{\beta^2 - \omega^2 \mu_0 \epsilon_3}}{\epsilon_1 \epsilon_2} \cos(\sqrt{\omega^2 \mu_0 \epsilon_2 - \beta^2} h)$$
(2.74)

CHAPTER 3 RESULTS

Validation of the dyadic Green's function was accomplished via both analytical and numerical techniques. First, we show analytically that our Green's function reduces to the Green's function for a current element radiating above a dielectric half space when the permittivity of medium 1 is made equal to the permittivity of region 2. We analyze each component of the dyadic Green's function in turn.

3.1 Analytical validation of dyadic Green's function

3.1.1 The Gxx and Gyy components

Consider the $R_{\alpha\alpha}(\mathbf{k},\mathbf{R})$ component of the Green's function:

$$R_{\alpha\alpha}(\mathbf{k}, \mathbf{R}) = \{ R_{21}^{t}(\mathbf{k}) R_{23}^{t}(\mathbf{k}) e^{-j2p_{2}(\mathbf{k})h} e^{-jp_{2}(\mathbf{k})(z-z')} + R_{23}^{t}(\mathbf{k}) e^{-jp_{2}(\mathbf{k})(z+z')}$$

$$+ R_{21}^{t}(\mathbf{k}) e^{-j2p_{2}(\mathbf{k})h} e^{jp_{2}(\mathbf{k})(z+z')}$$

$$+ R_{21}^{t}(\mathbf{k}) R_{23}^{t}(\mathbf{k}) e^{-j2p_{2}(\mathbf{k})h} e^{jp_{2}(\mathbf{k})(z-z')} \} \frac{e^{j\mathbf{k}\cdot(\rho-\rho')}}{2(2\pi)^{2}\epsilon_{2}p_{2}(\mathbf{k})(1-R_{21}^{t}(\mathbf{k})R_{23}^{t}(\mathbf{k})e^{-j2p_{2}(\mathbf{k})h})}$$

$$(3.1)$$

$$R_{mn}^{t}(\mathbf{k}) = \frac{p_{m}(\mathbf{k}) - p_{n}(\mathbf{k})}{p_{m}(\mathbf{k}) + p_{n}(\mathbf{k})}$$
(3.2)

Let the permittivity of region 1 be made equal to the permittivity of region 2. Then $p_1(\mathbf{k})$ becomes equal to $p_2(\mathbf{k})$ and :

$$R_{21}^{t}(\mathbf{k}) = \frac{p_{2}(\mathbf{k}) - p_{1}(\mathbf{k})}{p_{1}(\mathbf{k}) + p_{2}(\mathbf{k})} = \frac{p_{1}(\mathbf{k}) - p_{1}(\mathbf{k})}{p_{1}(\mathbf{k}) + p_{1}(\mathbf{k})} = 0$$
(3.3)

Substituting for $R_{21}^t(\mathbf{k})$ into (3.1):

$$R_{\alpha\alpha}(\mathbf{k}, \mathbf{R}) = \frac{R_{23}^{t}(\mathbf{k})e^{-j\mathbf{p}_{2}(\mathbf{k})(z+z')}e^{j\mathbf{k}\cdot(\rho-\rho')}}{2(2\pi)^{2}\epsilon_{2}p_{2}(\mathbf{k})}$$
(3.4)

Adding the principal portion to the reflected part we arrive at the total tangential component:

$$G_{\alpha\alpha}(\mathbf{k}, \mathbf{R}) = \frac{e^{-jp_2(\mathbf{k})|z-z'|} + R_{23}^t(\mathbf{k})e^{-jp_2(\mathbf{k})(z+z')}e^{j\mathbf{k}\cdot(\rho-\rho')}}{2(2\pi)^2\epsilon_2p_2(\mathbf{k})}$$
(3.5)

This expression agrees with that given in the Nyquist class notes, pp. 6-21 [12].

3.1.2 The Gzx and Gzy components

Consider the $R_{z\alpha}(\mathbf{k},\mathbf{R})$ component of the Green's function:

$$\begin{split} R_{z\alpha}(\mathbf{k},\mathbf{R}) &= k_{\alpha} \frac{1}{2(2\pi)^{2} \epsilon_{2} p_{2}(\mathbf{k})} [\\ &\{ \frac{N_{21}^{2} - 1}{p_{2}(\mathbf{k}) + N_{21}^{2} p_{1}(\mathbf{k})} R_{23}^{n}(\mathbf{k}) T_{21}^{t}(\mathbf{k}) e^{-j2p_{2}(\mathbf{k})h} \\ &+ \frac{(N_{32}^{2} - 1)}{p_{3}(\mathbf{k}) + N_{32}^{2} p_{2}(\mathbf{k})} R_{21}^{t}(\mathbf{k}) T_{23}^{t}(\mathbf{k}) e^{-j2p_{2}(\mathbf{k})h} \} e^{-jp_{2}(\mathbf{k})(z-z')} \\ &+ \{ \frac{N_{21}^{2} - 1}{p_{2}(\mathbf{k}) + N_{21}^{2} p_{1}(\mathbf{k})} R_{23}^{n}(\mathbf{k}) T_{21}^{t}(\mathbf{k}) R_{23}^{t}(\mathbf{k}) e^{-j2p_{2}(\mathbf{k})h} \\ &+ \frac{N_{32}^{2} - 1}{p_{3}(\mathbf{k}) + N_{32}^{2} p_{2}(\mathbf{k})} T_{23}^{t}(\mathbf{k}) \} e^{-jp_{2}(\mathbf{k})(z+z')} \\ &+ \{ \frac{N_{21}^{2} - 1}{p_{2}(\mathbf{k}) + N_{21}^{2} p_{1}(\mathbf{k})} T_{21}^{t}(\mathbf{k}) e^{-j2p_{2}(\mathbf{k})h} \\ &+ \frac{N_{32}^{2} - 1}{p_{3}(\mathbf{k}) + N_{32}^{2} p_{2}(\mathbf{k})} R_{21}^{t}(\mathbf{k}) R_{21}^{n}(\mathbf{k}) T_{23}^{t}(\mathbf{k}) e^{-j4p_{2}(\mathbf{k})h} \} e^{jp_{2}(\mathbf{k})(z+z')} \\ &+ \{ \frac{N_{21}^{2} - 1}{p_{2}(\mathbf{k}) + N_{21}^{2} p_{1}(\mathbf{k})} R_{23}^{t}(\mathbf{k}) T_{21}^{t}(\mathbf{k}) e^{-j2p_{2}(\mathbf{k})h} \\ &+ \frac{N_{32}^{2} - 1}{p_{3}(\mathbf{k}) + N_{32}^{2} p_{2}(\mathbf{k})} T_{23}^{t}(\mathbf{k}) R_{21}^{n}(\mathbf{k}) e^{-j2p_{2}(\mathbf{k})h} \} e^{jp_{2}(\mathbf{k})(z-z')}] \\ &- \frac{e^{j\mathbf{k}\cdot(\rho-\rho')}}{(1 - R_{21}^{n}(\mathbf{k}) R_{23}^{n}(\mathbf{k}) e^{-j2p_{2}(\mathbf{k})h}) (1 - R_{21}^{t}(\mathbf{k}) R_{23}^{t}(\mathbf{k}) e^{-j2p_{2}(\mathbf{k})h})} \end{split}$$

$$R_{mn}^{t}(\mathbf{k}) = \frac{p_{m}(\mathbf{k}) - p_{n}(\mathbf{k})}{p_{m}(\mathbf{k}) + p_{n}(\mathbf{k})}$$
(3.7)

$$T_{mn}^{t}(\mathbf{k}) = \frac{2p_{m}(\mathbf{k})}{p_{m}(\mathbf{k}) + p_{n}(\mathbf{k})}$$
(3.8)

$$R_{ml}^{n}(\mathbf{k}) = \frac{N_{lm}^{2} p_{m}(\mathbf{k}) - p_{l}(\mathbf{k})}{N_{lm}^{2} p_{m}(\mathbf{k}) + p_{l}(\mathbf{k})}$$

$$(3.9)$$

Let the permittivity of region 1 be made equal to the permittivity of region 2. The contrast ratio between layer 1 and 2 is:

$$N_{12}^2 = \frac{\epsilon_1}{\epsilon_2} = \frac{\epsilon_1}{\epsilon_1} = 1 \tag{3.10}$$

Again, the reflection coefficient between layer 1 and 2 vanishes thus:

$$R_{21}^{n}(\mathbf{k}) = \frac{N_{12}^{2}p_{2}(\mathbf{k}) - p_{1}(\mathbf{k})}{N_{12}^{2}p_{2}(\mathbf{k}) + p_{1}(\mathbf{k})} = \frac{p_{1}(\mathbf{k}) - p_{1}(\mathbf{k})}{p_{1}(\mathbf{k}) + p_{1}(\mathbf{k})} = 0$$
(3.11)

Also, the transmission coefficient between region 1 and 2 becomes unity:

$$T_{21}^{t}(\mathbf{k}) = \frac{2p_{2}(\mathbf{k})}{p_{1}(\mathbf{k}) + p_{2}(\mathbf{k})} = \frac{2p_{2}(\mathbf{k})}{2p_{2}(\mathbf{k})} = 1$$
 (3.12)

Making the appropriate substitutions into (3.6):

$$R_{z\alpha}(\mathbf{k}, \mathbf{R}) = k_{\alpha} \frac{1}{2(2\pi)^{2} \epsilon_{2} p_{2}(\mathbf{k})} \frac{N_{32}^{2} - 1}{p_{3}(\mathbf{k}) + N_{32}^{2} p_{2}(\mathbf{k})} T_{23}^{t}(\mathbf{k}) \cdot \exp(-j p_{2}(\mathbf{k})(z + z') + j \mathbf{k} \cdot (\rho - \rho'))$$
(3.13)

Adding the principal portion to the reflected part we arrive at the total Green's function component:

$$G_{z\alpha}(\mathbf{k}, \mathbf{R}) = k_{\alpha} \frac{1}{2(2\pi)^{2} \epsilon_{2} p_{2}(\mathbf{k})} \{ e^{-jp_{2}(\mathbf{k})|z-z'|} + \frac{N_{32}^{2} - 1}{p_{3}(\mathbf{k}) + N_{32}^{2} p_{2}(\mathbf{k})} T_{23}^{t}(\mathbf{k}) e^{-jp_{2}(\mathbf{k})(z+z')} \} e^{j\mathbf{k}\cdot(\rho-\rho')}$$
(3.14)

This expression agrees with that given in the Nyquist class notes, pp. 6-22 [12].

3.1.3 The Gzz component

Consider the $R_{zz}(\mathbf{k}, \mathbf{R})$ component of the Green's function:

$$R_{zz}(\mathbf{k}, \mathbf{R}) = \frac{1}{2(2\pi)^{2} \epsilon_{2} p_{2}(\mathbf{k})} [R_{21}^{n}(\mathbf{k}) R_{23}^{n}(\mathbf{k}) e^{-j2p_{2}(\mathbf{k})h} e^{-jp_{2}(\mathbf{k})(z-z')}$$

$$+ R_{23}^{n}(\mathbf{k}) e^{-jp_{2}(\mathbf{k})(z+z')} + R_{21}^{n}(\mathbf{k}) e^{-j2p_{2}(\mathbf{k})h} e^{jp_{2}(\mathbf{k})(z+z')}$$

$$+ R_{21}^{n}(\mathbf{k}) R_{23}^{n}(\mathbf{k}) e^{-j2p_{2}(\mathbf{k})h} e^{jp_{2}(\mathbf{k})(z-z')}] \frac{e^{j\mathbf{k}\cdot(\rho-\rho')}}{1 - R_{21}^{n}(\mathbf{k}) R_{23}^{n}(\mathbf{k}) e^{-j2p_{2}(\mathbf{k})h}}$$

$$(3.15)$$

$$R_{ml}^{n}(\mathbf{k}) = \frac{N_{lm}^{2} p_{m}(\mathbf{k}) - p_{l}(\mathbf{k})}{N_{lm}^{2} p_{m}(\mathbf{k}) + p_{l}(\mathbf{k})}$$

$$(3.16)$$

Let the permittivity of region 1 be made equal to the permittivity of region 2. Then $p_1(\mathbf{k})$ becomes equal to $p_2(\mathbf{k})$ and :

$$R_{21}^{n}(\mathbf{k}) = \frac{N_{12}^{2}p_{2}(\mathbf{k}) - p_{1}(\mathbf{k})}{N_{12}^{2}p_{2}(\mathbf{k}) + p_{1}(\mathbf{k})} = \frac{p_{1}(\mathbf{k}) - p_{1}(\mathbf{k})}{p_{1}(\mathbf{k}) + p_{1}(\mathbf{k})} = 0$$
(3.17)

Substituting for $R_{12}^n(\mathbf{k})$ into (3.1):

$$R_{zz}(\mathbf{k}, \mathbf{R}) = \frac{R_{23}^{n}(\mathbf{k})e^{-jp_2(\mathbf{k})(z+z')}e^{j\mathbf{k}\cdot(\rho-\rho')}}{2(2\pi)^2\epsilon_2p_2(\mathbf{k})}$$
(3.18)

Adding the principal portion to the reflected part we arrive at the total tangential component:

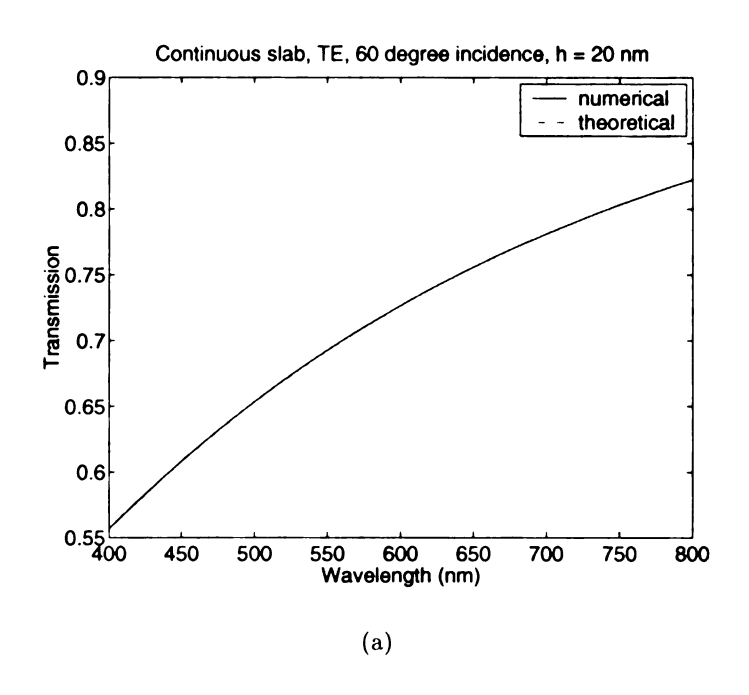
$$G_{zz}(\mathbf{k}, \mathbf{R}) = \frac{e^{-jp_2(\mathbf{k})|z-z'|} + R_{23}^n(\mathbf{k})e^{-jp_2(\mathbf{k})(z+z')}e^{j\mathbf{k}\cdot(\rho-\rho')}}{2(2\pi)^2\epsilon_2 p_2(\mathbf{k})}$$
(3.19)

This expression agrees with that given in the Nyquist class notes, pp. 6-21 [12].

3.2 Numerical validation of dyadic Green's function

We validate our dyadic Green's function numerically using the integral equation formulation described previously. We first generate a brick shaped mesh of height h_g and width w_g . At the same time, we specify the thickness of the background slab to

be h_1 and the period $D_x = D_y = w_g$. The volume equivalence principle allows us to replace the meshed region of the background slab with free space. Thus, we are able to analyze reflection and transmission from a slab of height $h = h_1 - h_g$. We compare the numerical solution to the analytical solution for a dielectric slab of height h. Specifically, we consider reflection and transmission from a dielectric slab as a function of thickness, incident angle, and wavelength. Figure 3.2 shows the transmission from two slabs of different height as a function of wavelength. Figure 3.2 displays transmitted intensity from a dielectric slab as a function of angle of incidence. We observe excellent agreement between analytical and numerical values.



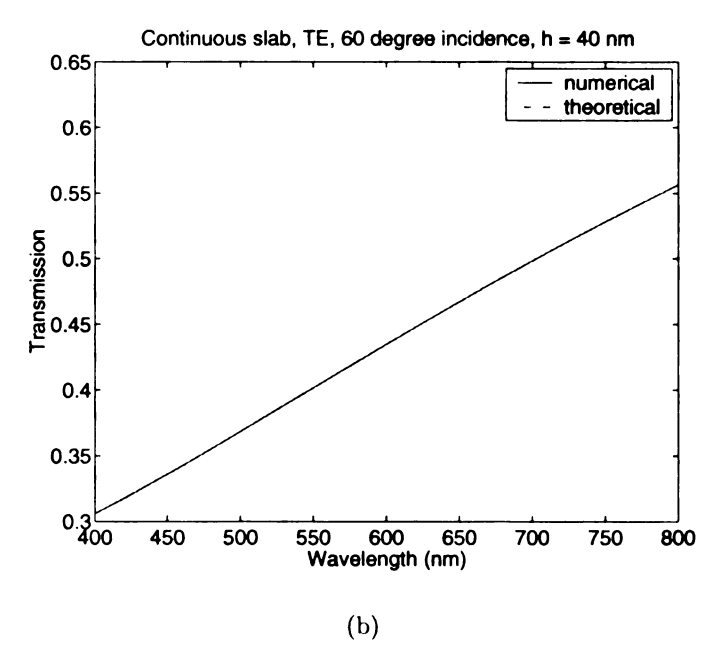


Figure 3.1 (a) Transmission from 20 nm slab of $\epsilon_r=4$ as a function of wavelength; (b) Transmission from 40 nm slab of $\epsilon_r=4$ as a function of wavelength

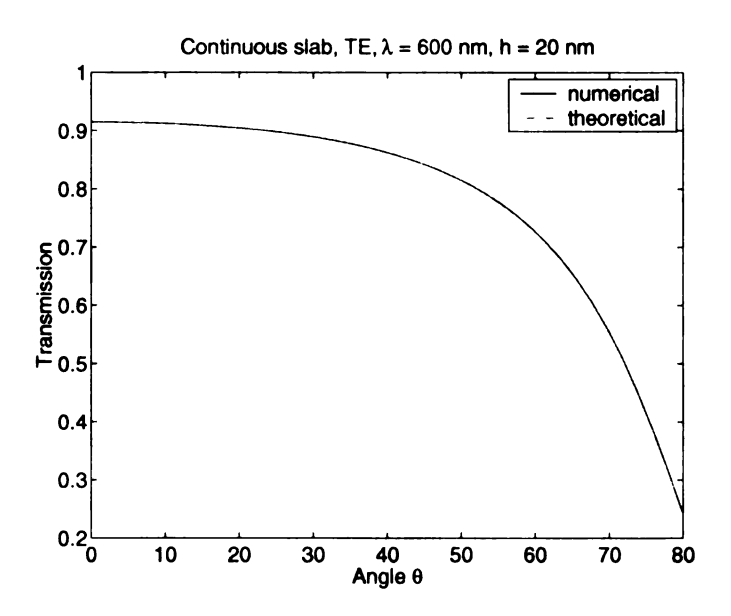


Figure 3.2 Transmission from 20 nm slab of $\epsilon_r=4$ as a function of angle

CHAPTER 4 CONCLUSION

In this thesis, we derived a spectral periodic Green's function for current elements radiating inside a layered medium. We introduced a volume integral equation formulation for electromagnetic (EM) scattering from arbitrarily shaped dielectric bodies in terms of unknown current **J**. A new derivation of the Green's function for a current element inside a single layer was presented. It was shown that this periodic Green's function could be calculated in the spectral domain provided that the Fourier integrals do not have poles on the real axis. A Kummer's transformation technique was used to improve convergence for source-observation pairs lying on either interface was discussed. We validated our Green's function via reduction to a canonical half-space problem. The periodic layered medium Green's function was validated numerically by comparison with analytical data for reflection and transmission from a single layer.

The periodic layered medium Green's function approach has two major computational advantages. As mentioned previously, the holes in a typical perforated metal only occupy roughly 5% of the area of the film. The layered medium approach allows us to mesh the hole region rather than the metal. Secondly, the periodic layered medium Green's function is evaluated inside the metal region. The large negative real permittivity causes the periodic layered medium Green's function to converge more quickly in the metal than in free space.

Future work will doubtless focus on analysis of larger structures. While our algorithm is much more efficient than conventional surface or volume integral equation formulations, the cost still scales as $\mathcal{O}(N^2)$. Fast methods such as the fast multipole method (FMM) or the adaptive integral method (AIM) need to be developed for layered media. Other interesting physics can be observed when one introduces multiple layers into the perforated thin film geometry. Our algorithm can be easily modified to accommodate substrate and superstrate layers.

APPENDIX A Components of dyadic Green's function

The tangential components $(\alpha = x, y)$ of the dyadic Green's function are given by:

$$\begin{split} R_{\alpha\alpha}(\mathbf{k},\mathbf{R}) &= \{R_{21}^{t}(\mathbf{k})R_{23}^{t}(\mathbf{k})e^{-j2p_{2}(\mathbf{k})h}e^{-jp_{2}(\mathbf{k})(z-z')} + R_{23}^{t}(\mathbf{k})e^{-jp_{2}(\mathbf{k})(z+z')} \\ &+ R_{21}^{t}(\mathbf{k})e^{-j2p_{2}(\mathbf{k})h}e^{jp_{2}(\mathbf{k})(z+z')} \\ &+ R_{21}^{t}(\mathbf{k})R_{23}^{t}(\mathbf{k})e^{-j2p_{2}(\mathbf{k})h}e^{jp_{2}(\mathbf{k})(z-z')}\} \frac{e^{j\mathbf{k}\cdot(\rho-\rho')}}{2(2\pi)^{2}\epsilon_{2}p_{2}(\mathbf{k})(1-R_{21}^{t}(\mathbf{k})R_{23}^{t}(\mathbf{k})e^{-j2p_{2}(\mathbf{k})h})} \end{split}$$

$$(A.1)$$

The normal components of the dyadic Green's function are given by:

$$\begin{split} R_{z\alpha}(\mathbf{k},\mathbf{R}) &= k_{\alpha} \frac{1}{2(2\pi)^{2} \epsilon_{2} p_{2}(\mathbf{k})} [\\ &\{ \frac{N_{21}^{2} - 1}{p_{2}(\mathbf{k}) + N_{21}^{2} p_{1}(\mathbf{k})} R_{23}^{n}(\mathbf{k}) T_{21}^{t}(\mathbf{k}) e^{-j2p_{2}(\mathbf{k})h} \\ &+ \frac{(N_{32}^{2} - 1)}{p_{3}(\mathbf{k}) + N_{32}^{2} p_{2}(\mathbf{k})} R_{21}^{t}(\mathbf{k}) T_{23}^{t}(\mathbf{k}) e^{-j2p_{2}(\mathbf{k})h} \} e^{-jp_{2}(\mathbf{k})(z-z')} \\ &+ \{ \frac{N_{21}^{2} - 1}{p_{2}(\mathbf{k}) + N_{21}^{2} p_{1}(\mathbf{k})} R_{23}^{n}(\mathbf{k}) T_{21}^{t}(\mathbf{k}) R_{23}^{t}(\mathbf{k}) e^{-j2p_{2}(\mathbf{k})h} \\ &+ \frac{N_{32}^{2} - 1}{p_{3}(\mathbf{k}) + N_{32}^{2} p_{2}(\mathbf{k})} T_{23}^{t}(\mathbf{k}) \} e^{-jp_{2}(\mathbf{k})(z+z')} \\ &+ \{ \frac{N_{21}^{2} - 1}{p_{2}(\mathbf{k}) + N_{21}^{2} p_{1}(\mathbf{k})} T_{21}^{t}(\mathbf{k}) e^{-j2p_{2}(\mathbf{k})h} \\ &+ \frac{N_{32}^{2} - 1}{p_{3}(\mathbf{k}) + N_{32}^{2} p_{2}(\mathbf{k})} R_{21}^{t}(\mathbf{k}) R_{21}^{t}(\mathbf{k}) T_{23}^{t}(\mathbf{k}) e^{-j4p_{2}(\mathbf{k})h} \} e^{jp_{2}(\mathbf{k})(z+z')} \\ &+ \{ \frac{N_{21}^{2} - 1}{p_{2}(\mathbf{k}) + N_{21}^{2} p_{1}(\mathbf{k})} R_{23}^{t}(\mathbf{k}) T_{21}^{t}(\mathbf{k}) e^{-j2p_{2}(\mathbf{k})h} \\ &+ \frac{N_{32}^{2} - 1}{p_{3}(\mathbf{k}) + N_{32}^{2} p_{2}(\mathbf{k})} T_{23}^{t}(\mathbf{k}) R_{21}^{n}(\mathbf{k}) e^{-j2p_{2}(\mathbf{k})h} \} e^{jp_{2}(\mathbf{k})(z-z')}] \\ &- \frac{e^{j\mathbf{k}\cdot(\rho-\rho')}}{(1 - R_{21}^{n}(\mathbf{k}) R_{23}^{n}(\mathbf{k}) e^{-j2p_{2}(\mathbf{k})h}) (1 - R_{21}^{t}(\mathbf{k}) R_{23}^{t}(\mathbf{k}) e^{-j2p_{2}(\mathbf{k})h})} \end{split}$$

where $\alpha = x, y$.

$$R_{zz}(\mathbf{k}, \mathbf{R}) = \frac{1}{2(2\pi)^{2} \epsilon_{2} p_{2}(\mathbf{k})} [R_{21}^{n}(\mathbf{k}) R_{23}^{n} e^{-j2p_{2}(\mathbf{k})h} e^{-jp_{2}(\mathbf{k})(z-z')}$$

$$+ R_{23}^{n} e^{-jp_{2}(\mathbf{k})(z+z')} + R_{21}^{n}(\mathbf{k}) e^{-j2p_{2}(\mathbf{k})h} e^{jp_{2}(\mathbf{k})(z+z')}$$

$$+ R_{21}^{n}(\mathbf{k}) R_{23}^{n} e^{-j2p_{2}(\mathbf{k})h} e^{jp_{2}(\mathbf{k})(z-z')}] \frac{e^{j\mathbf{k}\cdot(\rho-\rho')}}{1 - R_{21}^{n}(\mathbf{k}) R_{23}^{n}(\mathbf{k}) e^{-j2p_{2}(\mathbf{k})h}}$$
(A.3)

$$R_{mn}^{t}(\mathbf{k}) = \frac{p_{m}(\mathbf{k}) - p_{n}(\mathbf{k})}{p_{m}(\mathbf{k}) + p_{n}(\mathbf{k})}$$
(A.4)

$$T_{mn}^{t}(\mathbf{k}) = \frac{2p_{m}(\mathbf{k})}{p_{m}(\mathbf{k}) + p_{n}(\mathbf{k})}$$
(A.5)

$$R_{ml}^{n}(\mathbf{k}) = \frac{N_{lm}^{2} p_{m}(\mathbf{k}) - p_{l}(\mathbf{k})}{N_{lm}^{2} p_{m}(\mathbf{k}) + p_{l}(\mathbf{k})}$$
(A.6)

BIBLIOGRAPHY

- [1] P.I Nikitin, A.A. Beloglazov, V.E. Kochergin, M.V. Valeiko, and T.I. Ksenevich, "Surface plasmon resonance interferometry for biological and chemical sensing," *Sens. Actuators B-Chem.*, 1999, v. 54, pp. 43-50.
- [2] A.A. Kruchinin and Y.G. Vlasov, "Surface plasmon resonance monitoring by means of polarization state measurement in reflected light as the basis of a DNA-probe optical sensor," Sens. Actuators B-Chem., 1996, v. 30, pp. 77-80.
- [3] M. Kretschmann and A. A. Maradudin, "Band structures of two-dimensional surface-plasmon polaritonic crystals," *Physical Review B*, 2002, v. 66, pp. 245408(8).
- [4] H. Ghaemi, T. Thio, and D. Grupp, "Surface plasmons enhance optical transmission through subwavelength holes," *Physical Review B*, 1998, v. 58, pp. 6779-6782.
- [5] S.A. Darmanyan and A.V. Zayats, "Light tunnelling via resonant surface plasmon polariton states and the enhanced transmission of periodically nanostructured metal films: an analytical study," *Physical Review B*, 2003, v. 67, pp. 035424.
- [6] W.C. Chew, "Waves and Fields in Inhomogenous Media," IEEE Press, 1990.
- [7] K.A. Michalski and D. Zheng, "Electromagnetic scattering and radiation by surfaces of arbitrary shape in layered media," *IEEE Transactions on Antennas and Propagation*, 1990, v. 38, pp. 335-344.
- [8] R. Mittra, A.F. Peterson, and S.L. Ray, "Computational Methods for Electromagnetics," New York, NY, IEEE Press, 1998.
- [9] D.M. Pozar and D.H. Schaubert, "Scan Blindness in Infinite Phased Arrays of Printed Dipoles," *IEEE Transactions on Antennas and Propagation*, 1984, v. 32, pp. 602-610.
- [10] M. Abramowitz and I. Stegun, "Handbook of Mathematical Functions," Dover, New York, 1964.
- [11] J. Bagby and D.P. Nyquist, "Dyadic Green's Functions for Integrated Electronic and Optical Circuits," *IEEE Transactions on Microwave Theory and Techniques*, 1987, v. 35, pp. 207-210.
- [12] D.P. Nyquist, Course Notes of ECE 929A, "Advanced Topics in Electromagnetics: Planar Waveguides and Circuits," Michigan State University, Fall 1994.

